

INTEGRAL EQUATION MODEL OF THE MARTIAN SURFACE LAYER FOR THE DETECTION OF BURIED ICE DEPOSITS IN SUPPORT OF THE INTERNATIONAL ICE MAPPING MISSION SYNTHETIC APERTURE RADAR

Rafael F. Rincon, James B. Garvin,
David Hollibaugh-Baker,
NASA/Goddard Space Flight Center,
Greenbelt MD, 20771, USA

Roger H. Lang,
and Jiaxing Yang
The George Washington University,
Washington DC, 20052, USA

ABSTRACT

This work implemented a 3-D Electromagnetic Scattering model to gain a better understanding in the observations of L- and P-band radar returns from the multi-layered Martian upper surface layer. The model is based on the Integral Equation Model (IEM) developed by Adrian Fung. Our model implementation treats the upper surface (regolith) layer as an inhomogeneous medium with irregular boundaries for a range of Martian surface and shallow subsurface scenarios. The model is well suited to study the near subsurface (upper 10 meters of surface sediments) ice detection capability of the L-band (32 cm wavelength) Synthetic Aperture Radar (SAR) planned for the international Mars Ice Mapping (I-MIM) mission launching later in the 2020s.

Index Terms— IEM, Martian ice, Regolith, SAR

1. INTRODUCTION

The near subsurface – the upper ten meters – of Solar System planets and asteroids contain key information important to planetary science and exploration [1], [2]. These upper layers may contain water ice deposits, buried fluvial channels, former lake deposits, caves, buried rock fragments or large boulders from asteroid impacts, or other resources. Particularly, in the dust-covered environments of Mars, it is critical to be able to investigate bedrock and search for buried features to assess in-situ resources and determine the geologic/climate history of the planet. There is evidence that water is present in the subsurface of Mars in the form of ice deposits, at depths ranging from a few centimeters to several kilometers [3] [4]. For example, relatively thick layers of water ice have been observed in escarpments on Mars by HiRISE (High Resolution Imaging Science Experiment [5]), extending from just below the top surface to tens of meters in depth, as shown in Figure 1. Some Martian ice resides a few centimeters below the surface as revealed by the Phoenix Mars Polar Lander [5] photograph shown in Figure's 1 inset.

The near-surface region is close enough to the surface to be accessible to human or robotic explorers and thus contains information key for future science-driven exploration and for the understanding of the surface evolution.

L-band and P-band Synthetic Aperture Radar (SAR)

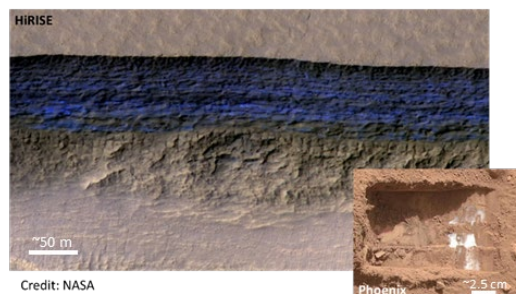


Figure 1. HiRISE image of Martian scarp shows a cross section of a thick sheet of underground ice (blue layer). Inset: Phoenix Mars Lander scooped regolith cover to reveal water ice just below the surface.

signals have the unique ability of penetrating meters into the upper subsurface, providing high spatial resolution (meter-scale) images of buried features [6],[7]. In addition, these types of radars do not suffer as severely from clutter interference (i.e., which can mask the radar signal returns from the upper subsurface) as the very low frequency HF and VHF profiling/sounding radars that are routinely used to probe much deeper depths (e.g., km to tens of km) below the surface. Furthermore, when these radar instruments employ polarimetry, their measurements provide information on the scattering mechanism of the interrogated regolith thus permitting the study of its vertical structure of the regolith and offering one means to by which distinguish or identify the type of buried medium (e.g., ice vs. bedrock).

Presently, however, there is an imperfect understanding of what the detection capabilities of low frequency (e.g., L- or P-band SAR) are for the broad variety of planetary surface deposits and subsurface layer compositions of interest. Hence, it is critical that accurate volumetric Electromagnetic (EM) Scattering models be evaluated for the different SAR measurements of Mars upper surface scenarios. Having this understanding is critical for the International-Mars Ice Mapper (I-MIM) mission, a proposed Mars orbital 930 MHz (referred here as L-band) SAR, being developed by NASA in collaboration with the Japan Aerospace Exploration Agency (JAXA), the Canadian Space Agency (CSA), and the Italian Space Agency (ASI), to inventory Mars' buried ice [8]. This understanding is equally important for the Space Exploration Synthetic Aperture Radar (SESAR), a prototype P-band (435 MHz) planetary SAR and mission concept, in development at

NASA Goddard Space Flight Center [9] for additional mission opportunities.

2. MODEL DESCRIPTION

Our implementation of the 3-D scattering model is based on the *Integral Equation Model* (IEM) developed by Adrian Fung and described in [10],[11], [12]. In our implementation, the interaction of SAR signals with the Martian upper layer is treated as a problem of electromagnetic wave propagation through a three-layer inhomogeneous medium with irregular boundaries. As illustrated in Figure 2, the top layer, representing the Martian atmosphere, is treated as empty space, and is characterized by the free space permittivity (ϵ_0) and permeability (μ_0). The middle layer, representing the Martian regolith, has a thickness or depth d_l and is characterized by an effective bulk permittivity (ϵ_l) and permeability (μ_l). This layer may be embedded with rock fragments of mean diameter d_f which are characterized by their own effective permittivity (ϵ_f) and permeability (μ_f), and which occupy a fractional volume V of the regolith layer. The layer is in turn bounded by a top, or ground, surface (S_1) and a bottom, or basal, surface (S_2). The bottom layer, representing either an ice layer or bed rock, is characterized by a permittivity (ϵ_2) and permeability (μ_2) and is considered a half-space with no additional scatterers.

The SAR observations of the Martian subsurface vary depending upon the polarization (q or p) of the radar signal, the top and bottom surface features, and the subsurface structure and composition. Surface “terrain” features, such as roughness and slope, determine how much of the radar signal scatters or penetrates the subsurface. The subsurface structure and composition determine, among other phenomena, the degree of volume scattering and the depth of penetration of the radar signal. The model’s top and bottom surfaces are characterized by their respective height standard deviation σ_1 and σ_2 , correlation length L_1 and L_2 , and correlation spectrums $w_1(L_1, \theta_1)$ and $w_2(L_2, \theta_2)$, where θ_1 and θ_2 are the local incidence angles on surfaces S_1 and S_2 , respectively.

As the radar transmits from orbit towards the planet’s surface located at a distance R from the radar antenna, the signal propagates spherically outward and behaves as a plane wave in the far field ($R \gg \lambda$). The incident electric field vector (\vec{E}_q^i) in the region of interest can be represented by $\vec{E}_q^i = \exp(i\mathbf{k} \cdot \vec{r})\vec{q}$, where \mathbf{k} is the wave vector, \vec{r} is a unit vector in the direction of the radar look angle, and \vec{q} is the signal polarization.

As the signal interacts with the top surface and the subsurface, it scatters and attenuates. The total scattered electric field (\vec{E}_p^s), where p (e.g., h or v) is the polarization of the scattered signal, is the sum of the scattering electric fields arising from the several field interactions, as shown in Figure 2. As a result, the total normalized radar backscattering cross-section (RBCS) observed by the radar is given by

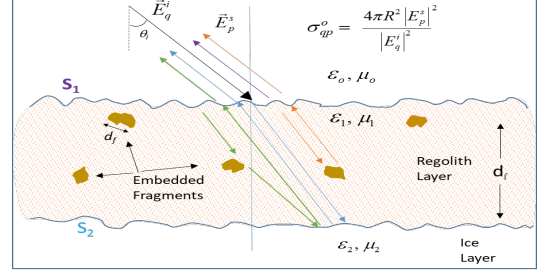


Figure 2. Three-dimensional electromagnetic scattering model for the observations radar returns from multi-layered inhomogeneous media with irregular boundaries.

$$\sigma_{qp}^o = \sigma_{S_1qp}^o + \sigma_{Vqp}^o + \sigma_{S_2qp}^o + \sigma_{V_{S_2}qp}^o, \quad (1)$$

where q and p represent the transmit and receive signal polarizations; and $\sigma_{S_1qp}^o$, σ_{Vqp}^o , $\sigma_{S_2qp}^o$ and $\sigma_{V_{S_2}qp}^o$ are the RBCS components from the regolith top surface, regolith volume, ice layer surface, and volume-ice layer surface interaction, respectively.

3. MARTIAN SCENARIOS UNDER CONSIDERATION

The EM modeling of the interaction of SAR signals with the Martian surface and shallow subsurface is primarily a function of the top and bottom surface roughness and slope, the layer composition and its electric and magnetic properties, and the radar’s signal frequency and local incidence angle. Measurements and images from orbiting sensors, landers, and rovers indicate that the Martian landscape varies widely in surface roughness and slope across most regions. Martian (northern) plains are likely the regions with most roughness variability, ranging from very smooth to significantly rough [13]. Images acquired by rovers and landers at different Martian locations over the years illustrate the variability (Fig. 3).

The regolith’s dielectric permittivity (Real part) depends on its temperature, geometric mineralogical composition, and porosity, and is proportional to the layer’s density in most cases. The value of the dielectric permittivity is presumed to be driven mainly by the layer bulk density and its range of values is relatively narrow [6]. In this analysis, the relative permittivity ($\epsilon_r = \epsilon / \epsilon_0$) values employed were: 4.48-0.0448i for the upper layer (regolith), 6.20-0.0005i for clastic rock



Figure 3. Martian landscape images captured by rovers and landers illustrate surface roughness variability in different regions of the planet. Credit: NASA.

fragments (e.g., basaltic), and $3.00 - 0.00015i$ for the buried water ice layer, which are consistent with general permittivity values found in the literature [7],[14]. The same permittivity values were used for both 930 MHz and 435 MHz calculations as these values are not expected to change significantly over this range frequencies. Magnetic properties of the layer constituents are not considered in this report, and, hence, the permeability employed in the model is the free space permeability μ_0 .

Table 1. Martian scenarios under consideration classified on the basis on subsurface ice detectability.

	High Detectability	Marginal Detectability
Top Surface	Smooth Roughness $\sigma < 1 \text{ cm}, L > 20 \text{ cm}$	High Roughness $\sigma \geq 1 \text{ cm}, L \leq 20 \text{ cm}$
Volume	$d_f < 1 \text{ cm}, FV < 1 \%$	$d_f \geq 1 \text{ cm}, FV \geq 1 \%$
Ice Surface	Pure ice, High Roughness $\sigma > 3 \text{ cm}, L < 20 \text{ cm}$	Pure Ice, Smooth Roughness $\sigma \leq 3 \text{ cm}, L \geq 20 \text{ cm}$

In this preliminary analysis, we consider three types of Martian surface and regolith scenarios classified on the basis of subsurface ice detectability: highly detectable and marginally detectable cases, as described in Table 1. The radar (SAR) signal local angle of incidence is 45° for all cases.

The high detectability scenario (case 1) is representative of regolith layers with relatively smooth top surfaces (compared to the signal wavelength), containing low fractional volume of rock fragments, and overlying a thick ice layer. These types of terrains are understood to exist in the Martian Northern hemisphere (35° to 55° N), where evidence of widespread water-ice buried below sand-like regolith has been suggested [3],[4]. The marginal detectability scenario (case 2) is representative of top rough surfaces -- due to rock fragment covered areas, as shown in Fig. 3, for example -- with moderate to high fractional volume of rock clasts within the regolith layer, having mean diameters greater than a centimeter.

The model makes several assumptions regarding the backscatter cross-section coefficient [11]. The first assumption is that only single scattering is present at both the surface and within the volume. This assumption is reasonable for the modeling of P- and L-band co-polarized components. The second assumption is that the transmission across the top surface can be accounted for by using the Fresnel transmission coefficients. This assumption is valid for low dielectric layers (e.g., ~ 2 to 5 for the Real part). The third assumption is that the reflection at the lower boundary for the surface-volume interaction term can be calculated using the Fresnel reflection coefficients. All these assumptions have been found to be acceptable for the Martian scenarios under consideration and agree with terrestrial results.

4. MODEL RESULTS

The total and individual RBCS components in (1) were computed as a function of ice layer depth for the three cases considered, as shown in Fig 4. A rough regolith-ice interface with an RMS height of 3 cm and a correlation length close to

half wavelength (parameters set for L-band. i.e., $L_2 = \lambda/2 = 16 \text{ cm}$ was used for all three cases for comparison purposes). The remainder of the parameters are set according to the criteria given in Table 1.

Moreover, since subsurface ice detection will rely on polarimetric SAR techniques for I-MIM, we implemented a “detectability test” to obtain a more quantifiable assessment of what the performance of a polarimetric SAR would be for Mars. This test provides a quantitative assessment of the “polarimetric” backscatter contribution from the bottom surface to the total polarimetric backscatter. The test employs the ratio of σ_{HH} to σ_{VV} to account for both co-polarized radar signal returns. The Total RBCS is the sum of the individual components as indicated in (1). For this test we compute the “No Ice” RBCS by subtracting the ice layer component from the total RBCS (or alternatively by locating the ice layer deep enough below the surface such that there are no observable radar returns from the bottom surface. Both approaches yield the same results). We then compute the *detectability metric* D as:

$$D = \left(\frac{\sigma_{totalHH}^o}{\sigma_{totalVV}^o} \right)_{dB} - \left(\frac{\sigma_{no\ iceHH}^o}{\sigma_{no\ iceVV}^o} \right)_{dB} . \quad (2)$$

Detectability metric plots for the two cases are shown in Figure 5.

The model results indicate that when the top surface is smooth and the regolith is free of embedded fragments (case 1; see Table 1 and in Figs. 4 and 5, *left columns*), the subsurface ice RBCS component is high relative to the top surface component. Since there are no embedded fragments in the regolith, no volume or volume-surface interaction components are present. The detectability test indicates that in this case the ice may be properly detected using polarimetric techniques up to around 6 m and 10 m depths at L- and P-band, respectively.

A transition between the two cases in Table 1 occurs when small fragments are present in the regolith at low fractional volumes and the top surface becomes slightly rougher. In this transition case (not shown in this paper for the sake of brevity), the ice surface RBSC component is still observable but the depth at which the ice layer is detectable decreases.

As top surface gets rougher, and the size and fractional volume of rock fragments in the regolith layer increase (case 2; see Table 1 and Figs. 4 and 5, *right columns*), the RBCS components from the top surface and regolith volume increase and the ice layer component decreases due to attenuation by the layer. In this case the ice layer returns are masked by the other components at most regolith layer depths, except at depths just below surface (e.g., $< 0.5 \text{ m}$ at L-band and $< 3 \text{ m}$ at P-band).

5. ACKNOWLEDGMENTS

This work was possible thanks to a grant by NASA and the support of I-MIM pre-Phase A Project. Special thanks to Dr. R. Davis for funding this work.

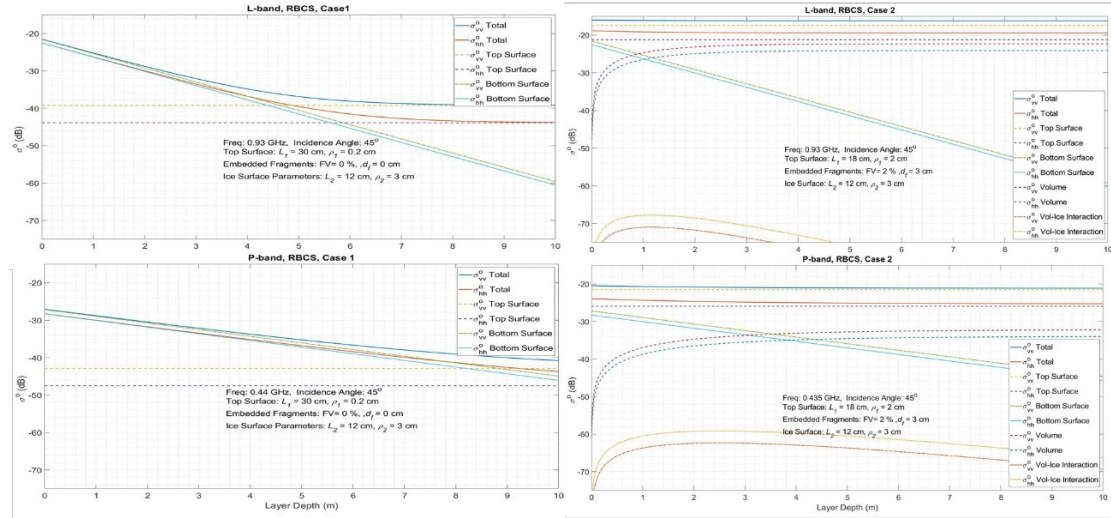


Figure 4 Martian Regolith modeling of RCBS components for L-band (top) and P-band (bottom) for the two cases presented.

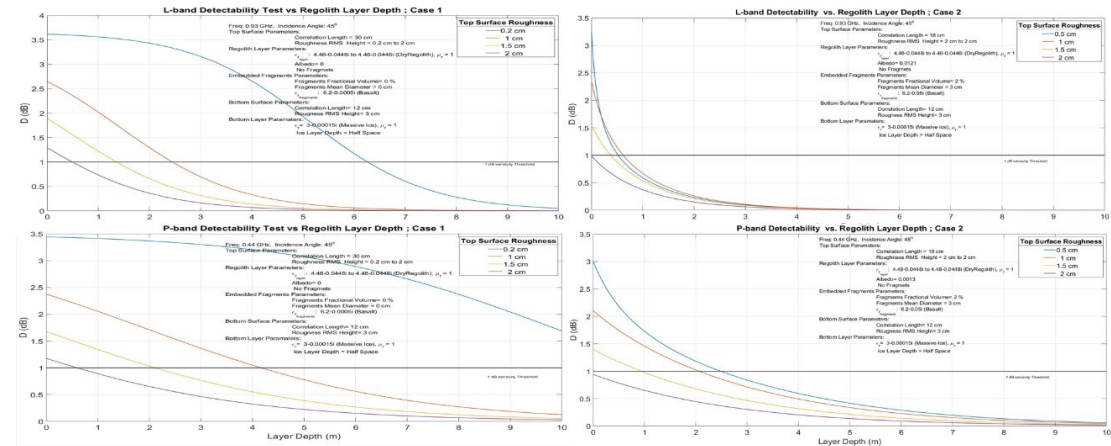


Figure 5 Detectability tests at L-band (top) and P-band (bottom) for the two cases presented.

6. REFERENCES

- [1] MEPAG NEX-SAG Report, Report from the Next Orbiter Science Analysis Group (NEX-SAG), Chaired by B. Campbell and R. Zurek, posted Dec. 2015 by MEPAG at <http://mepag.nasa.gov/reports.cfm>
- [2] The Lunar Exploration Roadmap: Exploring the Moon in the 21st Century: Themes, Goals, Objectives, Investigations and Priorities. White paper posted 2015 by the Lunar Exploration Program Analysis Group (LEAG), 2016.
- [3] Piqueux, S., et al. "Widespread shallow water ice on Mars at high latitudes and mid latitudes." *Geophys. Res. Lett.* 46 (2019): pp. 14290-14298.
- [4] Dundas C., Bramson A., Ojha L., et al., "Exposed subsurface ice sheets in the Martian mid-latitudes." *Science* Vol 359, no. Issue 6372 (Jan 2018): 199-201.
- [5] NASA Missions, NASA, Dec 13, 2021. [Online]. Available: <https://www.nasa.gov/missions>
- [6] B. A. Campbell, T. A. Maxwell, and A. Freeman. "Mars orbital synthetic aperture radar: Obtaining geologic information from radar polarimetry." *Journal of Geophysical Research*, Vol. 109 (2004).
- [7] P. Paillou, Y. Lasne, E. Heggy, et al., "A study of P-band synthetic aperture radar applicability and performance for Mars exploration: Imaging subsurface geology and detecting shallow moisture." *Journal of Geophysical Research* 11, no. e6 (2006).
- [8] NASA, International Partners Assess Mission to Map Ice on Mars, Guide Science Priorities, posted Feb. 2021 at <https://www.nasa.gov/feature/nasa-international-partners-assess-mission-to-map-ice-on-mars-guide-science-priorities>.
- [9] R. F. Rincon, L. M. Carter, R. Banting, et al., "Recent developments of the space exploration synthetic aperture radar (SESAR) for planetary science missions", *Geoscience and Remote Sensing Symposium (IGARSS)*, 2021, doi: 10.1109/IGARSS47720.2021.9554080.
- [10] A. K. Fung, *Microwave Scattering and Emission Models and Their Applications*, Norwood MA, USA, Artech House, 1994.
- [11] A. K. Fung and K. S. Chen, *Microwave Scattering and Emission Models for Users*. Norwood, MA: Artech House, 2010.
- [12] J. Yang, R. Lang, R. Rincon, and J. Garvin, "Backscattering from Martian Regolith Layer over an Underlying Half Space of Water/Ice", in *URSI Radio Science*, Jan. 2021, p. 29. URSI 2021.
- [13] R.A. Simpson, J.K. Harmon, S. Zisk, T.W. Thompson. and D. Muhleman. *Radar Determination of Mars Surface Properties*. Tucson, AZ: University of Arizona Press, 1992.
- [14] Ciarletti V, Clifford S, Plettemeier D, et al. The WISDOM Radar: Unveiling the Subsurface Beneath the ExoMars Rover and Identifying the Best Locations for Drilling. *Astrobiology*. 2017;17(6-7):565-584. doi:10.1089/ast.2016.1532